Methodology for collapse fragility development for hurricane events: electrical transmission towers

Xinlong Du[1] and Jerome F. Hajjar[2]

[1]Graduate Research Assistant, Department of Civil and Environmental Engineering, Northeastern University, Boston, MA 02115, USA (corresponding author). Email: du.xinl@northeastern.edu

[2]CDM Smith Professor and Chair, Department of Civil and Environmental Engineering, Northeastern University, Boston, MA 02115, USA. Email: jf.hajjar@northeastern.edu

ABSTRACT

This paper introduces a methodology for developing collapse fragility curves for windstorms, with a focus on assessing collapse of transmission towers for hurricane events. Incremental dynamic analysis (IDA) that incorporates the entire hurricane duration is adopted for collapse modeling. Fragility curves are cumulative distribution functions of a structural limit state such as collapse capacity, which is designated in this work as the intensity measure associated with the onset of collapse. A suite of selected hurricane wind records are used with IDA to propagate uncertainties from wind speeds, directions, and durations to collapse capacities. Compared with earthquake engineering methodologies, this work proposes appropriate approaches for scaling of wind records, fitting of IDA curves from simulation data, and parameter estimation of hurricane fragility curves. Fragility curves are appropriate for use both to quantify uncertainty in the context of performance-based wind design and for regional loss assessments. As inelastic deformations are allowed in performance-based wind design, it is useful to develop fragility curves based on nonlinear time history analysis for the entire windstorm duration, which has not been addressed in prior work.

Keywords: fragility, collapse, full-duration hurricanes, transmission tower, incremental dynamic analysis

1. Introduction

As structural engineers are moving towards performance-based wind design, geometric nonlinear and inelastic responses of structures are increasingly being accounted for in design (ASCE 2023; Barbato et al. 2013; Chuang and Spence 2019, 2020). Nonlinear time history analysis (NLTHA) may be adopted to assess structural performance and thus demonstrate that inelastic deformations are controlled. Given that nonlinear dynamic analysis is path dependent, NLTHA may be needed for a long duration to represent a windstorm fully. To facilitate performance-based wind design, fragility curves can be used to estimate the conditional probability of failure given a wind hazard intensity. Fragility curves can be developed through conducting NLTHA for a suite of representative wind events. However, there is little prior work on 1) characterizing windstorms with a suite of wind records that can capture the nature of the windstorms for the purpose of performance-based wind design, and 2) predicting dynamic structural responses subjected to a suite of wind records with long or full windstorm durations of hours to days (ASCE 2023). To address the first issue, Du et al. (2023) worked on hurricanes and developed a wind map that can provide a suite of representative hurricane wind speed and direction records for a specific location. This work focuses on the second problem, in which a methodology is developed for creating collapse fragility curves using NLTHA for full-duration hurricanes. Electrical transmission towers subjected to hurricane wind records selected using the approach presented by Du et al. (2023) are presented as an example application.

Fragility curves are used to describe the relationship between the failure probability of a structure and the intensity measure of the applied hazard. To calculate the failure probability of a structure for a certain intensity level of hazard is a standard structural reliability problem, where the uncertainties may come from structural properties and hazards with the same intensity level but other different characteristics. Therefore, each point on a fragility curve can be obtained from a structural reliability analysis. Depending on the uncertainties considered in the limit state function, there are time-invariant reliability and time-variant reliability. Consequently, fragility curves can also be developed based on time-invariant reliability or time-variant reliability.

For the time-invariant reliability approach, the limit state function can be expressed as $g(\boldsymbol{X})$, where $\boldsymbol{X}$ is a set of random variables. The fragility is defined as the failure probability of the structural system conditional on the specified intensity measure IM, i.e., $P(g(\boldsymbol{X}) \leq 0|IM)$. To satisfy the precondition of time-invariant reliability, one should assume the loads are static or consider the dynamic effects implicitly through some amplification factors. For example, Ellingwood et al. (2004) and Li (2005) developed hurricane fragility curves for light-frame wood construction using design equations with static wind pressure and a gust-effect factor to account for the maximum dynamic response. The conditional failure probabilities that form the fragility curves were obtained by increasing the wind speed in 10 mph increments and repeating the first-order reliability method (FORM) at each increment. The results were also used to validate the two-parameter lognormal cumulative distribution function (CDF) model of fragility curves by a series of statistical analyses (Li 2005; Li and Ellingwood 2006), which shows that the lognormal CDF provides a good model for fragility curves of light-frame wood construction. Shanmugam (2011) also developed fragility curves for roof uplift capacities in low-rise residential construction by using static wind loads, but considered correlated non-normal random variables. Shanmugam (2011) accepted the idea that the fragility can be modeled as a lognormal CDF, so Shanmugam did not use FORM or any other reliability methods to calculate failure probabilities, but combined Monte Carlo simulation and the maximum likelihood method suggested by Shinozuka et al. (2000) to estimate the two parameters of the lognormal CDF. Similarly, Shafieezadeh et al. (2013) and Darestani et al. (2022) assumed static wind loads with gust-effect factors according to ASCE 7 (ASCE 2010, 2016) and developed fragility curves for utility wood poles and transmission towers, respectively. However, the gust-effect factor is developed for structural design and assumes that the structure remains linear elastic. Therefore, the design equations with a gust-effect factor may not be suitable for highly nonlinear collapse failure analysis.

For the time-variant reliability approach, the failure event is described with respect to a time domain. For example, a time-variant reliability problem may be defined with a limit state function $g(\boldsymbol{X}, \boldsymbol{Y}(t))$, where $\boldsymbol{Y}(t)$ represents a set of random processes such as time histories of wind speeds and ground motions. For a certain time t, $\boldsymbol{Y}(t)$ becomes a set of random variables; therefore, the instantaneous failure probability at time t may be obtained through the approaches for calculating time-invariant reliabilities. Traditionally, the failure probability is asked to be estimated over the duration of an event, which is the first-passage problem and can be addressed by using a series system approximation after discretizing the duration into a series of successive short time intervals or by estimating the mean rate of down-crossings of the random process $g(\boldsymbol{X}, \boldsymbol{Y}(t))$ below zero (Der Kiureghian 2005). A more practical time-variant reliability problem may be defined by a limit state function $g(\boldsymbol{X}, \boldsymbol{Y}(0)\sim\boldsymbol{Y}(t))$, which means that the instantaneous failure event at time t depends on the random processes $\boldsymbol{Y}(t)$ from time 0 to t. For example, due to the dynamic effects and plastic deformations, the structure's response at time t dependents on the force time history from 0 to t; thus, the failure probability at time t dependents on the force time history from 0 to t. The method of series system approximation may be used to solve the problem as was done for the limit state function $g(\boldsymbol{X}, \boldsymbol{Y}(t))$; however, the correlations of failures between different time intervals during the duration of an event need to be considered (Der Kiureghian 2005; Kim et al. 2013; Kim et al. 2019; Song and Ok 2010). For the limit state function $g(\boldsymbol{X},\ \boldsymbol{Y}(0)\sim\boldsymbol{Y}(t))$, if only the failure probability after an event (i.e., at the end of the loading time history) is of interest, Monte Carlo simulation may be used to account for the uncertainties from random processes $\boldsymbol{Y}(t)$. For fragility development, a set of time history analyses may be run using different $\boldsymbol{Y}(t)$'s to propagate the uncertainties from $\boldsymbol{Y}(t)$ to structural responses. This is the common way to develop fragility curves in earthquake engineering, where the failure probability provided by fragility curves is for seismic events, and fragility curves are usually developed using nonlinear time history analysis with a suite of ground motions. However, collapse fragilities for full-duration windstorm events such as hurricanes and tornados have not been introduced into wind engineering. This is probably due to the massive computational demand to run nonlinear time history analyses for windstorms, whose durations are much longer than earthquakes.

In the context of fragility development for transmission towers under wind loads, researchers attempted to develop analytical fragility curves using static analysis (Cai et al. 2019; Darestani et al. 2022) or dynamic analysis with fixed time intervals such as 2 minutes (Ma et al. 2021; Tian et al. 2020), 5 minutes (Fu et al. 2016), and 10 minutes (Fu et al. 2020). The fragilities developed for these time intervals cannot represent the fragilities for a whole windstorm event because wind speeds and directions may vary during a storm, and failure of a structure incorporates accumulating phenomena such as yielding and dynamic effects. When using these fragility curves, the duration of a windstorm is discretized into a series of short time intervals (e.g., 2 minutes), and the failure probability is calculated for each time interval independently. However, as discussed before, the failure probabilities for those short time intervals are correlated (Der Kiureghian 2005; Straub et al. 2020). This correlation is difficult to quantify from the view of time-variant reliability and is not considered by the above authors. Hallowell et al. (2018) used the 1-hour peak wind record to represent a whole hurricane and tried to develop fragility curves for a hurricane event. For this case, except for the problem that the structure may be damaged before the 1-hour peak wind record, another problem here is that the 1-hour peak wind record is not necessarily the worst hour within a storm. For example, for a transmission tower the wind direction of the 1-hour peak wind record may be parallel to conductors and thus the wind forces on conductors may be negligible, while there may be a worse hour which has a lower wind speed but a wind direction perpendicular to the conductors.

To overcome the above-mentioned limitations of the current fragility development strategies for wind loads, this research tries to develop fragilities for full-duration windstorm events and focuses on collapse of transmission towers subjected to hurricanes. The limit state function has a form of $g(\boldsymbol{X},\ \boldsymbol{Y}(0) \sim \boldsymbol{Y}(t))$ since nonlinear and dynamic effects are included in collapse modeling. Instead of assessing failure probabilities for a series of time intervals within a hurricane, the research tries to estimate the failure probability after a hurricane event so that users can avoid the intractable task of quantifying correlations of failure probabilities in different time intervals. The storm-maximum 3-second gust wind speed is adopted as the intensity measure of hurricanes, and a suite of hurricane wind speed and direction records are selected to represent the uncertainties in wind loading (Du et al. 2023). The collapse limit state is considered through incremental dynamic analysis (IDA) adapted from earthquake engineering (Vamvatsikos and Cornell 2002), from which the collapse capacity (i.e., the intensity measure associated with the onset of collapse) is obtained. Prior work in the literature that used IDA for capacity assessment of transmission towers under wind loading includes Banik et al. (2010), Mara (2013), and Zhang et al. (2015); however, the wind records used for IDA are not for storm events and only have 35-second, 1-min or 5-min time intervals with a constant wind direction, which still have difficulties in dealing with the correlations of failure probabilities for different time intervals over the duration of an event. In this work, IDA is performed with a suite of full-duration hurricane wind records so that the results can be used for developing fragilities for hurricane events. The parameter estimation approaches for fragility curves are introduced for cases where the collapse capacity points for all wind records are completely or partially captured on IDA curves. Finally, a methodology is proposed for developing collapse fragility curves for transmission towers in a region using its specific towers and hurricane wind records.

2. Uncertainties in hurricane wind records

It is well-known that hurricane wind records with the same intensity measure may have different patterns or uncertainties in terms of the changing of wind speeds and directions. In fragility analysis, these uncertainties should be modeled and propagated to structural responses. The record-to-record uncertainties can be considered through Monte Carlo simulation, which requires running IDAs for a suite of hurricane wind records collected for a location of interest. To achieve this goal, Du et al. (2023) used Massachusetts as a testbed, discretized it into a series of grids (Fig. 1), and collected hurricanes wind records for each grid from a 10,000-year synthetic hurricane catalog (Liu 2014). However, due to the high computational demand, it is intractable to use all the collected wind records (about 200 for each grid, some of which may have durations on the order of 10 hours) for IDAs and fragility development. A subset of the collected records is used in this work, while still preserving the key uncertainties in the loading. This is achieved through clustering of the wind records and selecting several of them from each cluster. Using a neural network autoencoder, Du et al. (2023) first compressed the high-dimensional wind records into low dimensional latent features through a encoder process. The latent features were then expanded to reconstruct the wind records through a decoder process. Training of this neural network was done to minimize the difference between the original and the reconstructed wind records. Consequently, the low-dimensional latent features contain the most important information in the wind records. Finally, a k-means clustering algorithm was used on the latent features, through which approximately 1/10 of the wind records were selected in each cluster for fragility development. As such, the number of wind records used to run IDAs for each grid is approximately 20. As an example, 16 selected hurricane wind records from 8 clusters are shown in Fig. 2 for Grid 86 whose centroid has a latitude of 41.7 and a longitude of -70.1. Here the wind velocities are resolved into the North and East directions because the wind records have changing wind directions. Specifically, the wind records are time series of wind velocity vectors in 2D with a 10-min time step. Therefore, the clustering and selection process considers the effects of wind durations, speeds, and directions, which are all reflected in the values of the latent features. In Fig. 2, the wind records selected from the same cluster are shown in the same color, and it is seen that wind records within the same cluster have similar characteristics in terms of wind speeds, directions, and durations. In addition, 1-hour ramp-up and ramp-down loading histories are added to the beginning and the end, respectively, of each wind record to avoid an impulse effect due to sudden loading (see Fig. 2) for the nonlinear structural dynamic analyses in the following sections (ASCE 2023). To better compare wind records from different clusters, wind records in Fig. 2 are put together with their midpoint of the duration occurring at the same time. To facilitate the autoencoder, zero paddings at the beginning and end of each record are used to make all records have the same duration in these plots; however, these zero paddings are removed in the following nonlinear dynamic analysis. As the hurricane wind records used for IDA have different durations, the uncertainties in hurricane wind durations are accounted for in the developed fragilities.

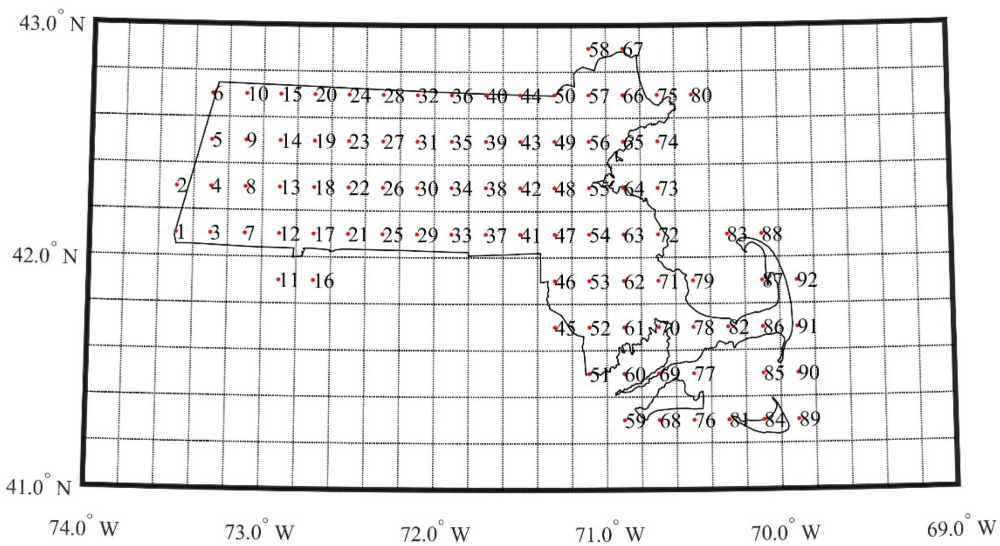

Fig. 1. Massachusetts is discretized into grids with their centroids shown and labelled

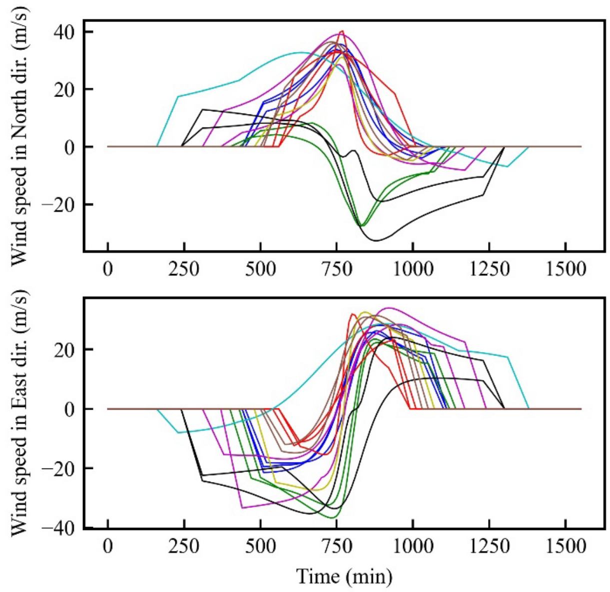

Fig. 2. An example of selected hurricane wind records for a grid

3. Hurricane wind loading on transmission towers

The selected hurricane wind records are 10-min mean wind speeds at 10 m height. To calculate the wind loads on transmission towers, the wind field along the towers should be generated, which includes modeling of the atmospheric boundary layer and the fluctuating wind speeds. The wind loading time histories may then be calculated based on the equations in the ASCE 74 design code (ASCE 2020).

3.1. Wind field simulation

As an example, Fig. 3 shows the step plot of a 10-min mean wind speed record at a 10 m height, along with the corresponding wind direction record. Note that the wind direction is clockwise positive from the North direction. Based on the 10-min mean wind speeds at 10 m height, the 10-min mean wind speeds at other heights along the tower are calculated according to the logarithmic law boundary layer model (Simiu et al. 1974; Simiu et al. 1976; Simiu and Scanlan 1996), which is

$$U(z) = \frac{u_*}{k} \ln \frac{z}{z_0} \tag{1}$$

where $U(z)$ is the mean wind speed at the height of z; u_* is the shear velocity; $k = 0.4$ is the Von Karman constant; z_0 is the roughness length of the ground surface. In this research, open terrain with a roughness length $z_0 = 0.03$ is assumed. After generating 10-min mean wind speeds for different heights, the fluctuating wind speeds should be superimposed to the mean wind speeds. Here the spatially correlated fluctuating wind speeds are simulated from the Kaimal spectrum (Kaimal et al. 1972) using the spectral representation method (Deodatis 1996; Shinozuka 1972; Shinozuka and Jan 1972). The correlations of fluctuating wind speeds at different locations are considered through a coherence function, which is an exponential decay as proposed by Davenport (1961). Fig. 4 presents the simulated and target spectra of the fluctuating wind speeds with a good match. The simulation of the fluctuating wind speeds is based on the open-source code developed by Cheynet (2020). After combining the mean and fluctuating wind speeds at different heights, the temporal-spatial evolution of the hurricane wind field along a transmission tower is obtained as presented in Fig. 5, where the seven wind records are for the seven different heights along a transmission tower as shown in Fig. A.1 of Appendix A (see both the red and blue dots in this figure). Only the absolute values of the wind speeds are shown in Fig. 5, while the changing of the wind directions are omitted for simplicity of the figure. Note that within each 10-min time interval, the wind direction is assumed to be constant even after adding the fluctuating wind speeds.

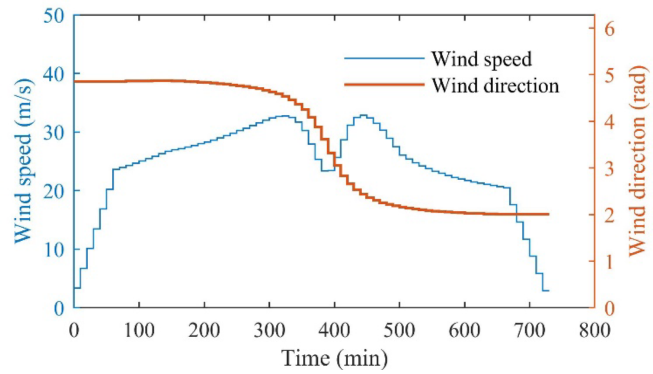

Fig. 3. An example of the 10-min mean wind speeds at 10 m height with the corresponding wind directions

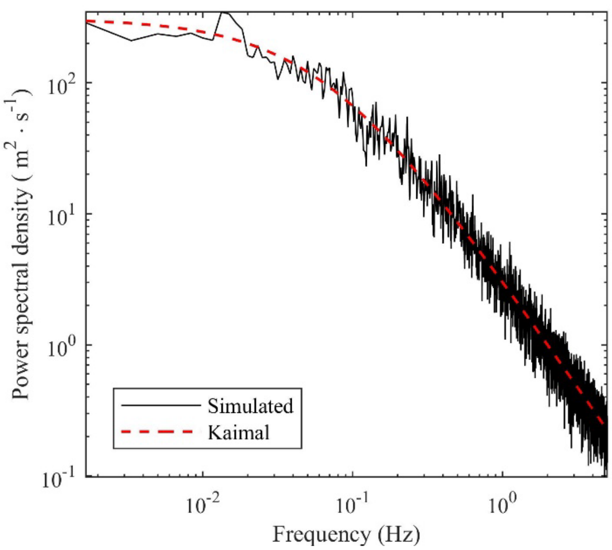

Fig. 4. Simulated and target spectra of fluctuating wind speeds

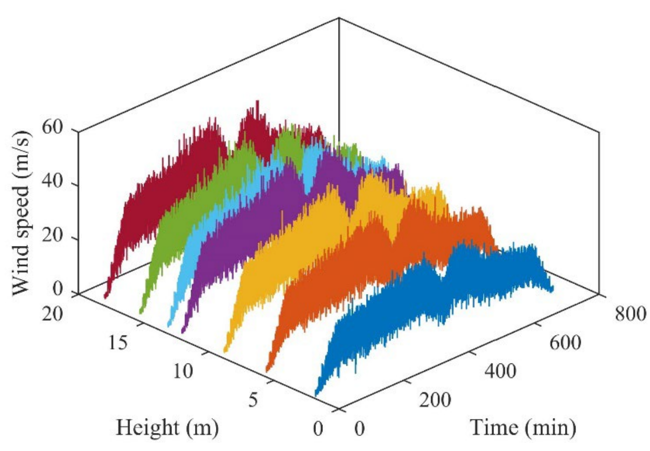

Fig. 5. Temporal-spatial evolution of synthetic hurricane wind speeds

3.2. Wind force calculation

Transmission towers are usually discretized into a series of panels along the height (Fig. 6), with wind forces calculated for each panel separately (Mara 2013). See Appendix A for details of the tower. Calculating wind forces necessitates the orientation of the tower, which is also the orientation of the conductors. These orientations are clockwise positive from the North direction, and the orientation of the tower in this example is assumed to be 0. This means the conductors and ground wires are running in the North-South direction. For transmission towers subjected to yawed wind, ASCE 74 (ASCE 2020) gives the following equation for wind force calculation on a lattice panel

$$F_d = QK_zK_{zt}{U_{3-sec}}^2G_t(1 + 0.2\sin^2(2\Psi))\left(C_{ft}A_{mt}\cos^2\Psi + C_{fl}A_{ml}\sin^2\Psi\right) \qquad (2)$$

where Q is the air density coefficient with a recommended value of 0.613 (m/s to Pa, converting wind speeds to pressure); K_z is the wind pressure exposure coefficient; K_{zt} is the topographic factor; G_t is the structure gust response factor; Ψ is the yaw angle as shown in Fig. 7; C_{ft} and C_{fl} are force coefficients associated with the face of the structure that is perpendicular to the transverse and longitudinal directions, respectively; and A_{mt} and A_{ml} are area of all members projected in the face of the structure that is perpendicular to the transverse and longitudinal directions, respectively. For conductors and ground wires subjected to yaw angles, ASCE 74 (ASCE 2020) gives the following equation for calculating wind forces perpendicular to the conductor or ground wire

$$F = QK_zK_{zt}{U_{3-sec}}^2G_wC_fA\cos^2\Psi \qquad (3)$$

where G_w is the wire gust response factor; C_f is the force coefficient with a recommended value of 1.0; and A is the projected area of the wire (i.e., wind span times the diameter of the wire). As recommended by Mara (Mara 2013), dynamic wind forces on the tower and wires are calculated using Eqs. (2) and (3) with the two terms $K_zK_{zt}{U_{3-sec}}^2G_t$ and $K_zK_{zt}{U_{3-sec}}^2G_w$ replaced by the simulated wind speeds at the corresponding height. As an example, Fig. 8 shows the calculated wind force time histories. Since the hurricane winds have time-variant wind directions, the wind forces are resolved into transverse and longitudinal directions for the ease to apply to the structure. Note that the two additional time histories in the transverse direction compared with those in the longitudinal direction are forces from one conductor and one ground wire.

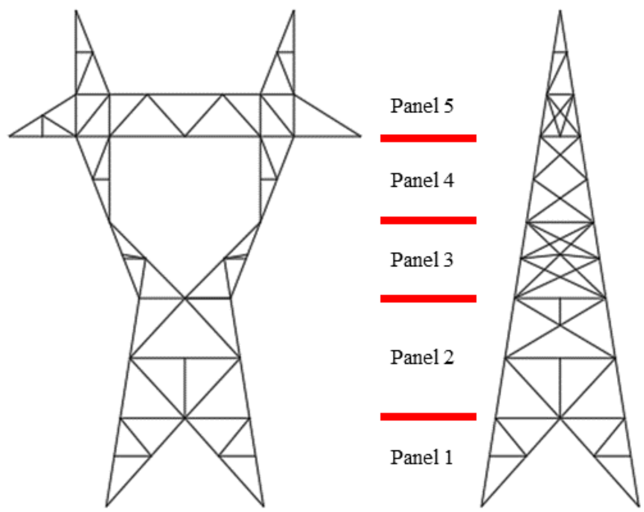

Fig. 6. An 18-m 115 kV transmission tower divided into panels

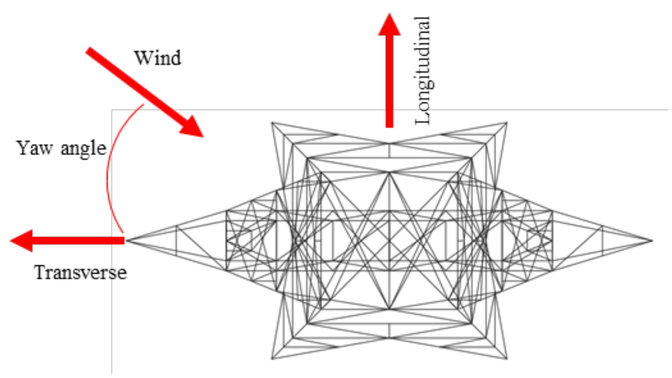

Fig. 7. Yawed wind on a transmission tower

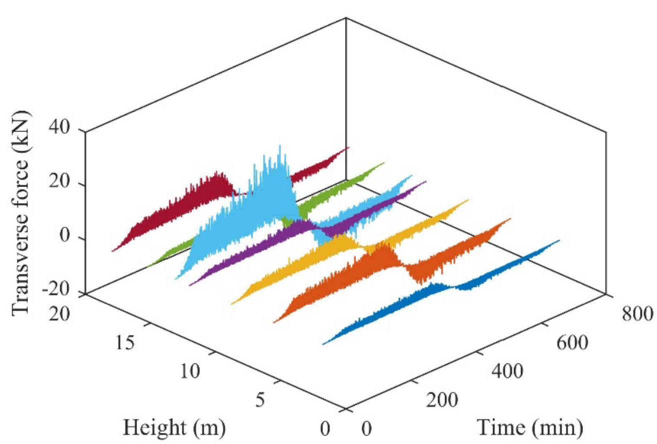

(a) Forces in the transverse direction

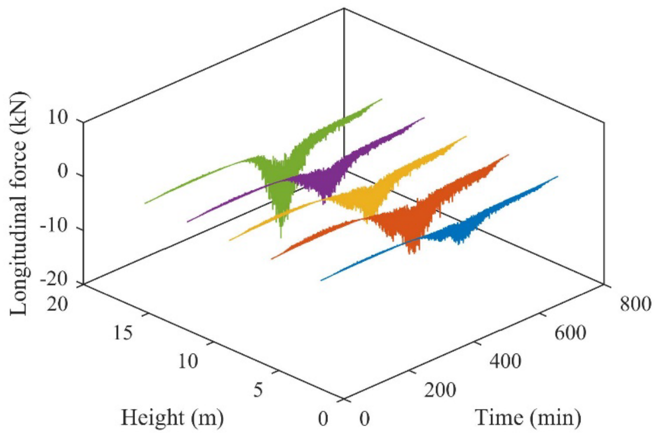

(b) Forces in the longitudinal direction

Fig. 8. Calculated wind forces on the transmission tower

4. Collapse fragility development

The collapse fragility curves are developed in this section for transmission towers under hurricanes. First, the mathematical model for fragility curves is briefly introduced. This section then discussed the details of using IDA to capture collapse capacities of towers subjected to the hurricane wind records selected in Section 2. The parameters of fragility curves are then estimated from the data of collapse capacities using the method of moments or the maximum likelihood method. Nonlinear dynamic analysis is done using the OpenSees software (McKenna et al. 2010) with the displacement-based beam element developed in Du and Hajjar (2021a, 2021b) for modeling structures made of steel angles and tees such as the transmission towers, where both material and geometric nonlinearities are considered. The axial-flexural-torsional interaction behavior is modeled for steel angles because they (including equal-leg angles) may experience flexural-torsional buckling under complex loading conditions like combined axial forces and moments (Liu and Hui 2008). The Newmark-beta method is used for the integrator with a time step of 0.05 seconds as suggested by Mara (2013) for transmission towers. The uniaxial Steel01 material in OpenSees is adopted with the nominal yield stress. Residual stress is modeled explicitly by applying the residual stress pattern suggested by Kitipornchai and Lee (1986) to fiber sections. Rayleigh damping is adopted with a 2% damping ratio. Other details of the finite element model in OpenSees can be found in Du and Hajjar (2022). The analyses for the IDAs were run on the DesignSafe cyberinfrastructure (Rathje et al. 2017).

4.1. Fragility curve and its parameter estimation

For the collapse limit state defined with a limit state function $g(\boldsymbol{X},\ \boldsymbol{Y}(0)\sim\boldsymbol{Y}(t))$, if the collapse capacity $IM_{collapse}$ is defined as the intensity measure associated with the onset of collapse for each sample of $\boldsymbol{Y}(t)$, the limit state function can be simplified as

$$g = IM_{collapse}\big(\boldsymbol{X}, \boldsymbol{Y}(0)\sim\boldsymbol{Y}(t)\big) - IM \tag{4}$$

Consequently, the fragility curve is the CDF of the random variable $IM_{collapse}$. This is because the conditional failure probability can be expressed as

$$P(g \le 0|IM) = P\big(IM_{collapse} \le IM\big|IM\big) \tag{5}$$

If it is assumed that $IM_{collapse}$ follows a lognormal distribution, then the fragility curve can be described as a lognormal CDF with two parameters, median θ and logarithmic standard deviation β. As used by many researchers (Ellingwood et al. 2004; Shinozuka et al. 2000), the fragility is defined as

$$F(IM) = \Phi\left(\frac{\ln(IM/\theta)}{\beta}\right) \tag{6}$$

where Φ denotes the standard normal CDF. The collapse capacity $IM_{collapse}$ is defined for a hurricane event and is obtained from IDA. This fragility can only describe the failure probability after an event instead of at any time during the event.

Parameter estimation for the fragility curves involves estimating values of the model parameters θ and β using the simulated data of the collapse capacity. Here the estimates of parameters θ and β are denoted as $\hat{\theta}$ and $\hat{\beta}$, respectively. Two methods are widely used for estimating the two parameters of fragility curves. The method of moments assumes that the resulting distribution and the simulated data have the same moments. The maximum likelihood method assumes that the resulting distribution makes the simulated data most probable (Baker 2015). Choosing of the parameter estimation method depends on the characteristics of the simulated data. The method of moments requires data set of the collapse capacity

$IM_{collapse}$, where parameters of fragility curves can be estimated from the simulated data by taking logarithms of each IDA curve's $IM_{collapse}$ value and calculating their mean and standard deviation (Baker 2015; Ibarra and Krawinkler 2005).

In addition to the traditional IDA, Baker (2015) also proposed a truncated IDA method, which means conducting IDA only up to some intensity level IM_{max}. This truncated IDA is used due to some concerns of scaling ground motions to very large IM levels: first, it is computationally intensive; second, the portions of fragility curves at very large IM levels are of less interest; third, the accuracy of using scaled ground motions with extreme IM levels to model the real highly intensive hazards is still questionable (Baker 2015). Here, similar concerns are also present in this research on hurricanes. Therefore, the truncated IDA is also investigated in this paper, which means the hurricane wind records are scaled only up to a relatively large and reasonable intensity level. If all n hurricane wind records used to run IDA cause collapse before the maximum intensity level, then the method of moments can be adopted for parameter estimation. Otherwise, if there are only m records ($m < n$) that cause collapse, the method of moments is no longer suitable and instead the maximum likelihood method presented in Baker (2015) is employed for parameter estimation. Specifically, the likelihood that the data set (m records cause collapse while (n-m) records does not) can be observed is shown as follows

$$Likelihood = \left[\prod_{i=1}^{m} \varphi\left(\frac{\ln(IM_{collapse,i}/\theta)}{\beta}\right)\right]\left[\prod_{j=1}^{n-m}\left(1-\Phi\left(\frac{\ln(IM_{max,j}/\theta)}{\beta}\right)\right)\right] \qquad (7)$$

where $\varphi()$ is the probability density function of the standard normal distribution; $IM_{collapse,i}$ is the $IM_{collapse}$ value for the i^{th} IDA curve; $IM_{max,j}$ is the maximum intensity level after scaling of the j^{th} wind record in the (n - m) records that did not cause collapse. Here, $IM_{max,j}$ is used because different wind records may be scaled up to different intensity levels, which is discussed in detail in Section 4.2. The two parameters θ and β can be evaluated by maximizing the likelihood function in Eq. (7) through an optimization algorithm. It is easier to maximize the logarithm of the likelihood function with getting a mathematically equivalent result, so the parameters can be estimated through

$$\{\hat{\theta}, \hat{\beta}\} = \underset{\theta,\beta}{\operatorname{argmax}} \sum_{i=1}^{m} \left[\ln \varphi \left(\frac{\ln(IM_{collapse,i}/\theta)}{\beta} \right) \right] + \sum_{j=1}^{n-m} \left[\ln \left(1 - \Phi \left(\frac{\ln(IM_{max,j}/\theta)}{\beta} \right) \right) \right] \quad (8)$$

4.2. Incremental dynamic analysis

In earthquake engineering, IDA is one common approach used to assess various limit states of structures, including global collapse capacity, where a suite of ground motions are scaled and applied to a structure in identifying the IM associated with the onset of collapse (Vamvatsikos and Cornell 2002). There are two main differences between IDA in wind engineering and earthquake engineering: one is the presence of mean and fluctuating wind speeds compared to the zero mean stochastic excitations of ground motions; another is the variation of the wind profile along the height of the structure (Mara 2013). To consider these differences, the 10-min mean wind speed records at 10 m height are first scaled for use in creating an IDA. The boundary layer model is then applied based on the scaled 10-min mean wind speed records at 10 m height to generate mean wind speeds at other heights, while the fluctuating wind speeds are generated and added to the mean wind speeds at different heights. For the scaling of ground motions, even though the efficient hunt-and-fill tracing algorithm (Vamvatsikos and Cornell 2002) has been introduced in prior years, researchers often prefer the simpler but more expensive algorithm of scaling up ground motions by a constant IM increment (Baker 2015). Similarly, this work also uses a constant increment of the storm-maximum 10-min mean wind speed for the scaling of wind records. Note that the mean wind speed records instead of the final records including the fluctuating wind speeds are scaled. This is because the generated fluctuating wind speeds depend on the corresponding mean wind speeds at the same location considering that the spectrum and the coherence function of the fluctuating wind speeds are functions of the mean wind speeds. Scaling of the final wind records including the fluctuating wind speeds may invalidate the Kaimal spectrum and the coherence function of the fluctuating wind speeds. Thus, the IM (i.e., storm-maximum gust speed) increment is not exactly but close to being constant due to the randomness of the fluctuating wind speeds. This also explains why a record-dependent $IM_{max,j}$ instead of a constant IM_{max} appears in Eqs. (7) and (8). Each scaled record is applied to the tower for nonlinear dynamic analysis. An example of the applied wind speeds and structural responses is shown in Fig. 9, where the sampling frequency is 100 seconds.

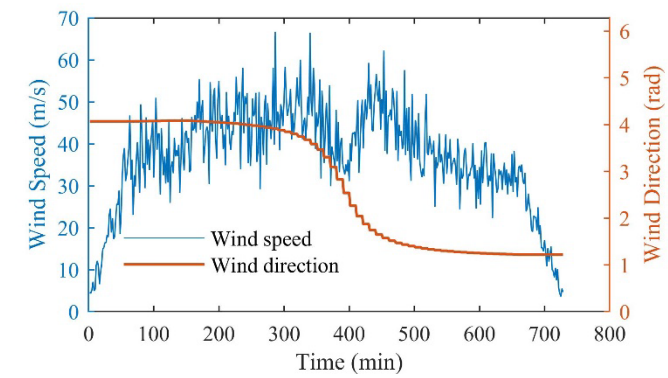

(a) Wind speeds and directions at 10 m height

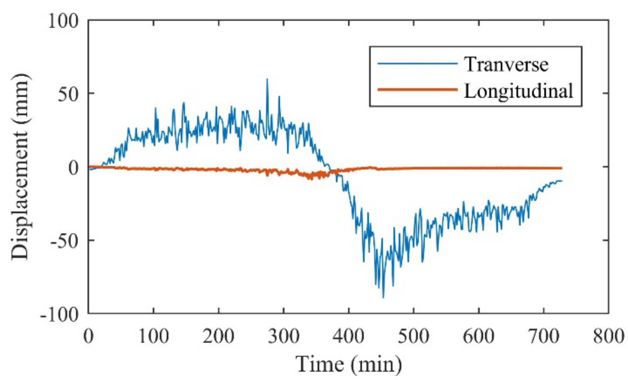

(b) Structural responses at the top of the tower

Fig. 9. Nonlinear dynamic analysis example

For transmission towers, the engineering demand parameter (EDP) is chosen as the peak displacement at the top of the tower. An IDA curve is a plot of EDP versus IM and Fig. 10 shows an example of the IDA curves using EDP as the horizontal axis and IM as the vertical axis. To develop this IDA curve, the storm-maximum 10-min mean wind speed of a hurricane wind record is scaled to be 10 m/s to 55 m/s with a 5 m/s increment. A total of 10 nonlinear dynamic analyses were performed, but the one with the most intensive wind record did not converge and is omitted in the figure. Here the Piecewise Cubic Hermite Interpolating Polynomial (PCHIP) (Fritsch and Carlson 1980; Kahaner et al. 1989) is employed to generate the IDA curve from the analysis points. Collapse is captured using the 20% slope criterion adapted from the *IM*-based rule in earthquake engineering (Vamvatsikos and Cornell 2002). As used in earthquake engineering, the onset of collapse is defined as the last point on the IDA curve with a tangent slope equal to 20% of the elastic slope (see the star in Fig. 10).

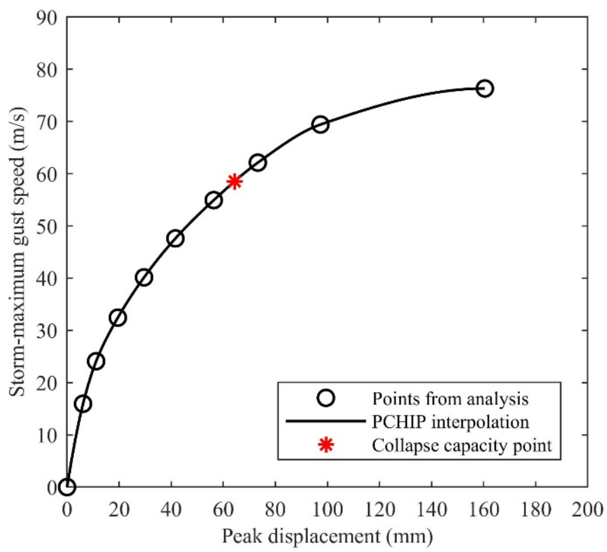

Fig. 10. An IDA curve generated using PCHIP interpolation and the corresponding collapse capacity point

Some prior work related to IDA recommends using spline interpolation to generate IDA curves (Vamvatsikos and Cornell 2002, 2004; Vamvatsikos et al. 2003). The authors found that the traditional 1D spline interpolation is not a good option to capture the collapse capacity point with the 20% slope criterion for hurricane response. The spline interpolation conducts cubic interpolation to construct piecewise polynomials with continuous second-order derivatives, which can be prone to oscillations and overshoots between data points (MathWorks 2022). Therefore, the authors propose to use the shape-preserving piecewise cubic interpolation, PCHIP, which only has continuous first-order derivatives and has no overshoots and fewer oscillations if the data points are not smooth. Specifically, the PCHIP interpolant is monotonic for intervals where the original data is monotonic. To demonstrate the superiority of the PCHIP interpolation for generating IDA curves, Fig. 11 (a) and (b) compare the IDA curves and collapse capacity points obtained from the same dataset but with a different number of data points. Eleven data points are generated through IDA. It is seen that when using all 11 data points, the PCHIP interpolation produces almost the same collapse capacity point as using the first 9 data points, while the spline interpolation produces a different collapse capacity point. For the spline interpolation case, the polynomials fitted from 9 data points and those fitted from 11 data points have significant differences in their first derivatives. If collapse happens between points 8 and 9, points 10 and 11 should be unnecessary. This is also important for a truncated IDA in which fewer data points from analysis are intended to provide similar collapse capacity as a corresponding IDA having more data points, as discussed in Section 4.1.

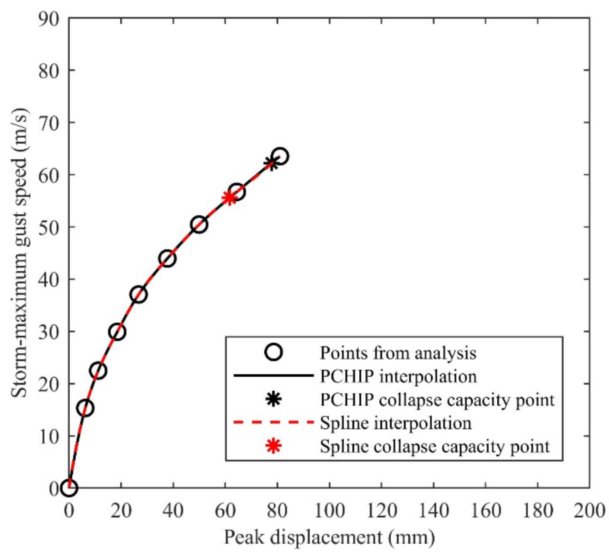

(a) Using 9 data points

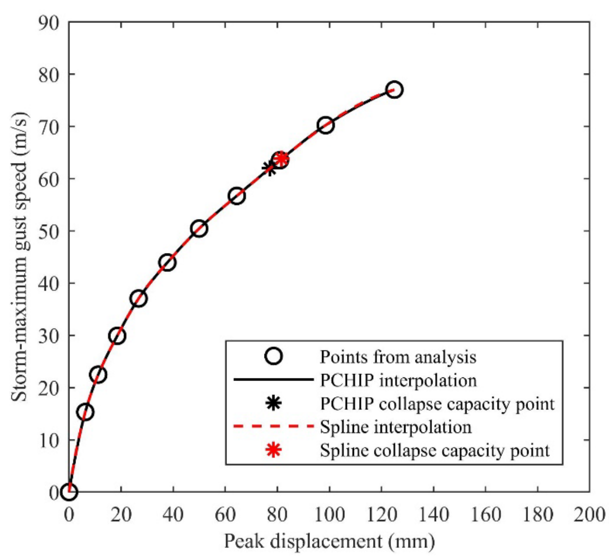

(b) Using 11 data points

Fig. 11. Comparison of the IDA curves and collapse capacity points from PCHIP and spline interpolations

4.3. Generation of fragility curves

To consider the uncertainties in hurricane wind speed and direction records, IDAs are run for a tower with a suite of wind records selected for the location of interest. If all wind records can produce collapse capacity values, then the method of moments is used for parameter estimation of fragility curves. On the contrary, if some of the records do not make the tower collapse until the maximum intensity level, they cannot produce collapse capacity values but can provide some lower bounds. This is designated a truncated IDA and the maximum likelihood method is used for parameter estimation. As an example, Fig. 12(a) illustrates 16 IDA curves with 16 collapse capacity points for the 115 kV tower shown in Fig. 6, while the corresponding fragility curve is developed using the method of moments. The result is shown in Fig. 12(b). Here the 16 hurricane wind records displayed in Fig. 2 are used and the storm-maximum 10-min mean wind speeds are scaled to be 10 m/s to 55 m/s with a 5 m/s increment. The nonconvergent computation results are not included in the figure. To demonstrate a truncated IDA, results from the highest two intensity levels are neglected for parameter estimation, which means the storm-maximum 10-min mean wind speed are scaled up to 45 m/s. Consequently, the 16 IDA curves can only produce 11 collapse capacity points as illustrated in Fig. 13(a). The corresponding fragility curve is estimated using the maximum likelihood method as in Eq. (8) and the result is shown in Fig. 13(b). It is seen that the truncated IDA can produce relatively accurate fragility curves with lower computational demand. Specifically, for this example the computational demand of a truncated IDA is 20% lower than a traditional IDA.

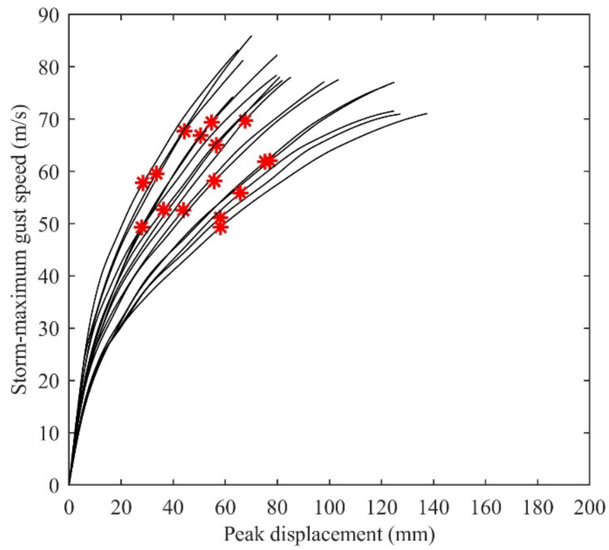

(a) IDA curves and the corresponding collapse capacity points (red stars)

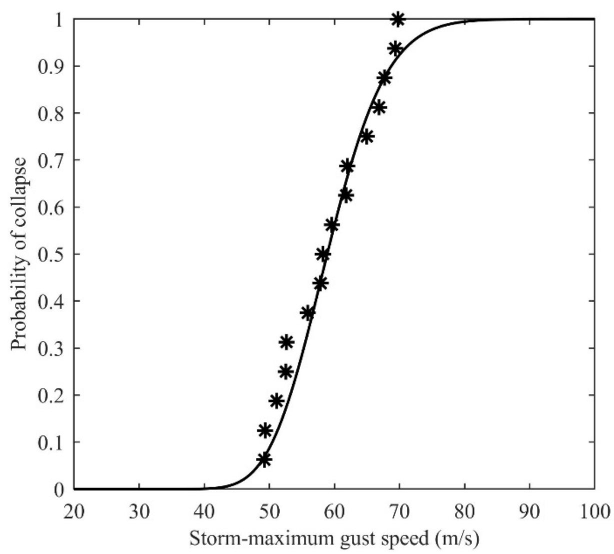

(b) Fragility curve estimated using the method of moment and the corresponding simulated data (black stars)

Fig. 12. Collapse fragility development using traditional IDA

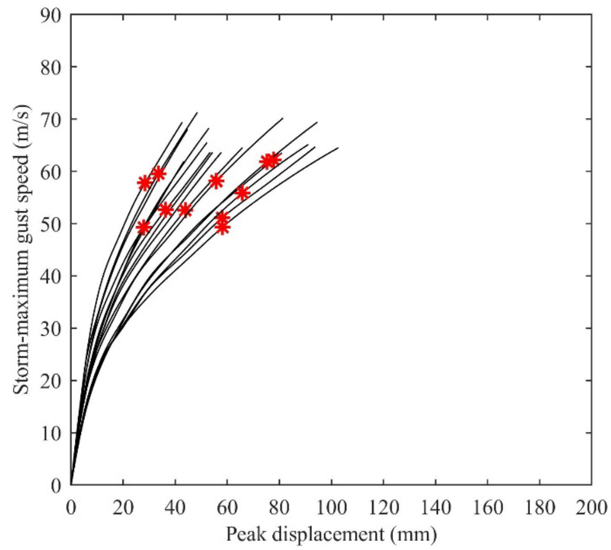

(a) IDA curves and the corresponding collapse capacity points (red stars)

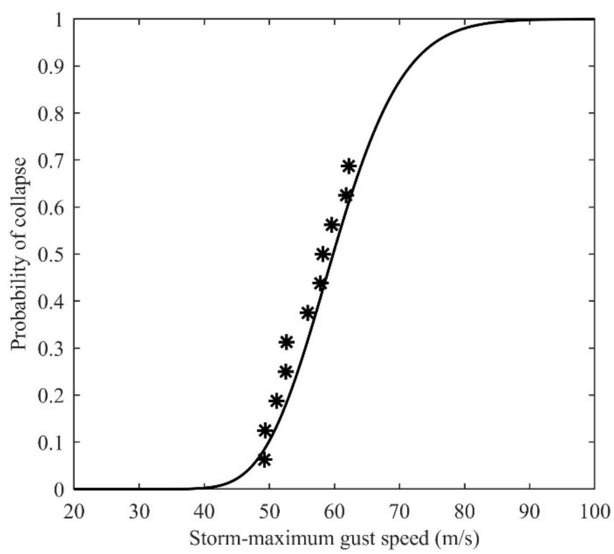

(b) Fragility curve estimated using the maximum likelihood method with the corresponding simulated data (black stars)

Fig. 13. Collapse fragility development using truncated IDA

The truncated IDA discussed earlier is due to the limit of the maximum intensity level. Sometimes an IDA may be truncated due to using a large increment of the intensity measure and the difficulty to converge the nonlinear dynamic analysis. If the analysis does not converge for some higher IM levels, the generated peak displacements for these IM levels should not be included in the IDA curve because they are not reliable. If the converged analyses with lower IM levels have not caused collapse, then this can be treated as a truncated IDA and all the nonconvergent analyses are ignored. Thus, the maximum likelihood method should be used for parameter estimation. For the j^{th} wind record, if the nonconvergent analysis starts from $IM_{k,j}$ in the k^{th} increment of the scaled wind records, then the one step lower value $IM_{k-1,j}$ will be used to replace the $IM_{max,j}$ in Eqs. (7) and (8). Theoretically, more accurate results can be obtained by performing more nonlinear dynamic analyses with IM levels between $IM_{k-1,j}$ and $IM_{k,j}$; however, using the truncated IDA as discussed here can be an alternative way considering the computational intensity of IDAs. In addition, if one is confident that the nonconvergence of the time integration can represent dynamic collapse, then the smallest nonconvergent intensity measure $IM_{k,j}$ will be a upper bound of $IM_{collapse}$ and a better parameter estimation can be achieved by replacing the term $\left(1-\Phi\left(\frac{\ln(IM_{max,j}/\theta)}{\beta}\right)\right)$ in Eqs. (7) and (8) with this new term $\left(\Phi\left(\frac{\ln(IM_{k,j}/\theta)}{\beta}\right)-\Phi\left(\frac{\ln(IM_{k-1,j}/\theta)}{\beta}\right)\right)$; however, this is not done in this work. These equations can be modified if within the development of a fragility curve some IDAs are truncated due to the limit of the maximum intensity level while some other IDAs are truncated due to nonconvergence.

5. Fragility development for a region

Fragility curves of transmission towers are essential for fast regional damage assessment of electrical transmission networks. Given the fact that characteristics of hurricane wind records are site-specific, fragility curves may be developed for towers at different locations. To demonstrate this idea, the geographic information of 115 kV overhead transmission lines in Massachusetts is collected from HIFLD open data and shown in Fig. 14. The same grids in Fig. 1 for hurricane wind records selection are used here to assign the transmission towers along the lines to their corresponding grids. In addition, since transmission towers are not axisymmetric, the orientation of a tower also has significant impacts on its collapse capacity and fragility curve. Theoretically, the orientation of towers can be obtained from the geographic data of transmission lines; however, developing fragility curves for all existing orientations is intractable due to the huge amount of computational demand. Thus, in this research towers are assumed to be doubly symmetric and fragility curves are only developed for five orientations, which are 0, π/8, π/4, 3π/8, and π/2.

Considering that the detailed information of towers is not publicly available, all towers in this 115 kV network are assumed to be the same as the one shown in Fig. 6, which may be unreasonable for practical applications but can be accepted here for a demonstration of the proposed methodology. To summarize, five fragility curves are developed for the 115 kV towers in each grid, and the selected hurricane wind records for each grid are employed to run IDAs. As an example, Fig. 15 plots fragility curves for the 115 kV towers with different orientations in two different grids, where the differences between the fragility curves in these two grids are due to the site-specific hurricane wind records. When using the fragility curves, the location and orientation of a tower should be determined first. An appropriate fragility curve may then be chosen from the developed fragility dataset. Since only five orientations are considered here, users can choose the fragility curve whose orientation is closest to the real orientation of the tower or apply interpolation techniques. The procedure described in this section is only a methodology, since the towers are only representative and cannot be used directly to assess the region of interest. Although only 115 kV transmission lines in Massachusetts are studied here, fragility curves of towers with other voltage levels can be developed using the same methodology.

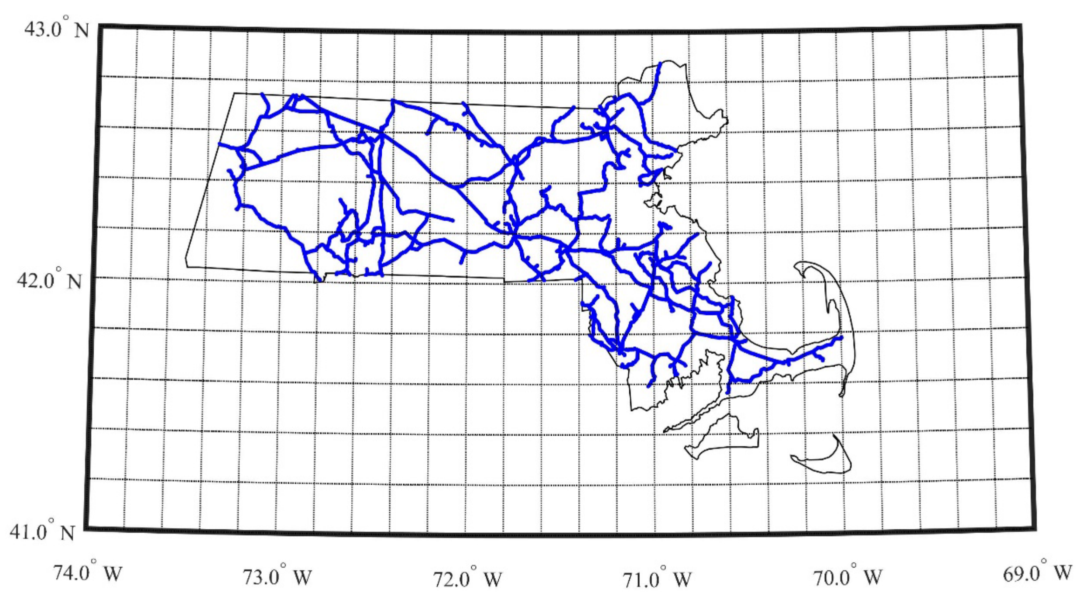

Fig. 14. Geographic information of 115 kV overhead transmission lines in Massachusetts

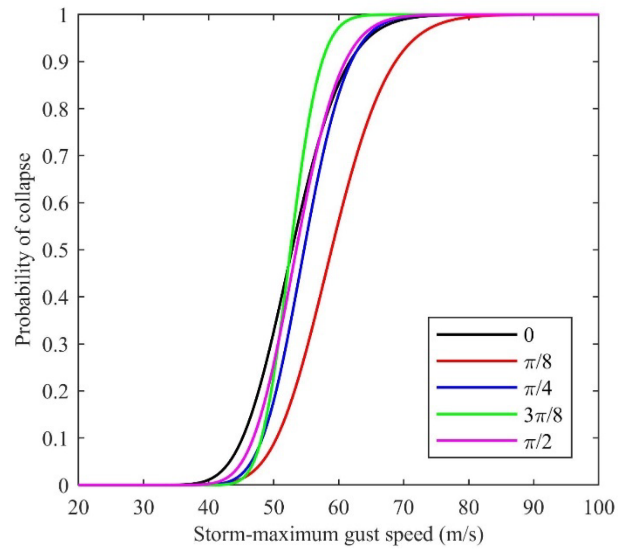

(a) Grid 86 with a centroid of latitude 41.7 and longitude -70.1

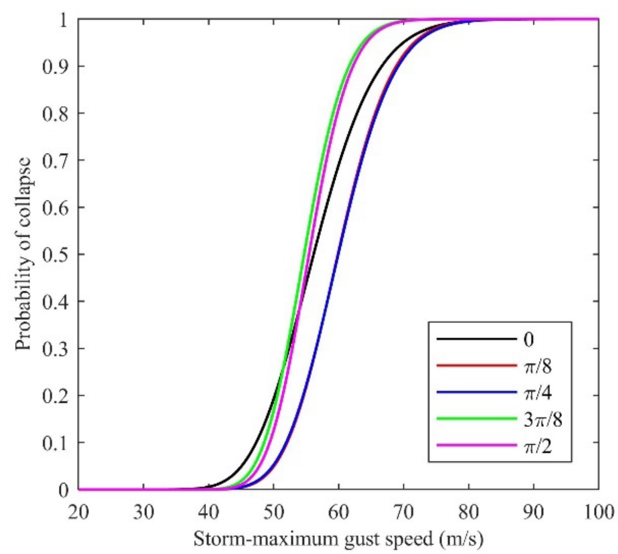

(b) Grid 78 with a centroid of latitude 41.7 and longitude -70.5

Fig. 15. Fragility curves for 115 kV towers with different orientations in two grids

6. Conclusions

This paper presents a methodology for developing collapse fragility curves for structures subjected to hurricanes and uses electrical transmission towers as an example application. The fragility curve describes the collapse probability of a structure after a hurricane event. Compared to the traditional wind fragilities developed for a fixed time interval, the fragilities for hurricane events can avoid the difficulty of quantifying the correlations of failure probabilities for different time intervals in the duration of an event. Uncertainties in hurricane wind speeds, directions, and durations are accounted for by assessing collapse capacities of transmission towers with a suite of hurricane wind records for a specific location. Both traditional IDA and truncated IDA are introduced to capture the collapse capacities with scaling of the hurricane wind records. The method of moments and the maximum likelihood method are adopted for parameter estimation of fragility curves based on the collapse capacity data obtained from IDA. Finally, a procedure for developing a set of fragility curves for a region is proposed and demonstrated with considerations of site-specific hurricane wind records and tower orientations. Performing IDAs for hurricane events is computationally intensive; however, as demonstrated in this paper, these analyses are feasible even for a large region with the currently available computation power. The methodology presented in this work can help in performance-based wind design for structures, and the developed fragilities for transmission towers can facilitate damage assessment of electrical transmission networks.

Data availability statement

Selected simulation cases including the OpenSees model of the tower studied in this paper are available at https://github.com/xinlong-du/TransTowerFragility.

Acknowledgement

The material presented in this paper is based upon work supported by National Science Foundation under Grant No. CRISP-1638234, the American Institute of Steel Construction, the American Iron and Steel Institute, the Metal Building Manufacturers Association, the Steel Deck Institute, the Steel Joist Institute, and Northeastern University. This support is gratefully acknowledged. This work used computational resources provided by the Natural Hazards Engineering Research Infrastructure: Cyberinfrastructure (DesignSafe), which is supported by National Science Foundation Grant No. CMMI-2022469. The authors wish to thank Dr. Weichiang Pang at Clemson University for providing the synthetic hurricane catalog and Robert Nickerson for his assistance with this research.

Appendix A. Transmission tower details

This appendix provides drawings of the 150 kV transmission tower used in this paper (Fig. A.1). Member sizes and design loads are given in Table A.1 and Table A.2, respectively.

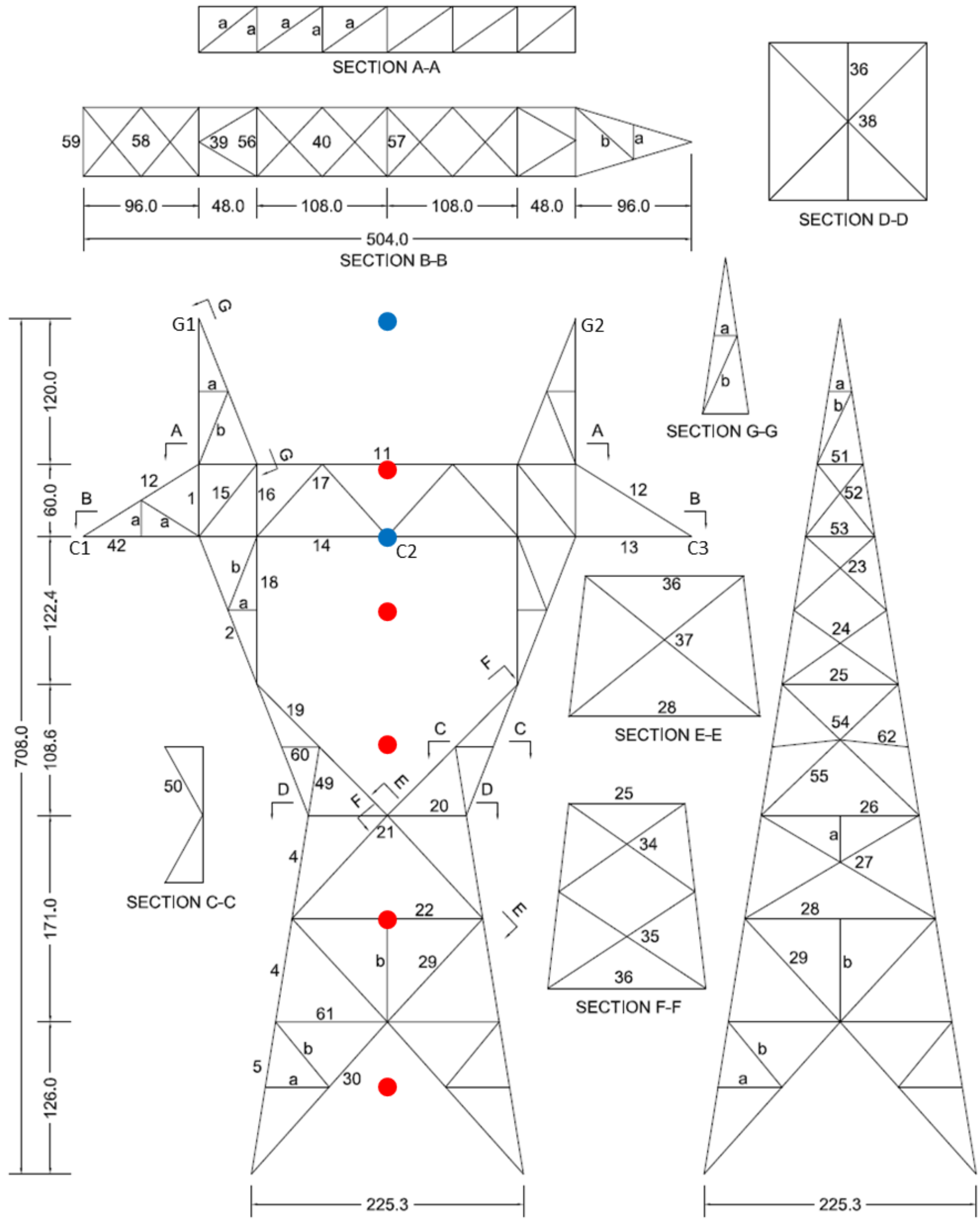

Notes: The red dots represent the heights of the wind records generated for each panel of the tower. The blue dots represent the heights of the wind records generated for conductors or ground wires.

Fig. A.1. Drawings of a 150 kV tower (units: inches)

Table A.1. Member sizes and materials of the tower in Fig. A.1

Member	Cross section (units: inches)	Material
1	$L3\frac{1}{2} \times 3\frac{1}{2} \times \frac{1}{4}$	A36
2	$L5 \times 5 \times \frac{3}{8}$	A572, Grade 50
3	$L5 \times 5 \times \frac{3}{8}$	A572, Grade 50
4	$L6 \times 6 \times \frac{7}{16}$	A572, Grade 50
5	$L6 \times 6 \times \frac{7}{16}$	A572, Grade 50
6	$L6 \times 6 \times \frac{7}{16}$	A572, Grade 50
7	$L6 \times 6 \times \frac{7}{16}$	A572, Grade 50
8	$L6 \times 6 \times \frac{7}{16}$	A572, Grade 50
9	$L6 \times 6 \times \frac{7}{16}$	A572, Grade 50
10	$L3 \times 3 \times \frac{3}{16}$	A36
11	$L4 \times 3\frac{1}{2} \times \frac{1}{4}$	A36
12	$L2\frac{1}{2} \times 2 \times \frac{3}{16}$	A36
13	$L4 \times 4 \times \frac{1}{4}$	A572, Grade 50
14	$L4 \times 3\frac{1}{2} \times \frac{5}{16}$	A572, Grade 50
15	$L4 \times 4 \times \frac{1}{8}$	A572, Grade 50
16	$L3\frac{1}{2} \times 3 \times \frac{1}{4}$	A572, Grade 50
17	$L4 \times 3\frac{1}{2} \times \frac{1}{4}$	A36
18	$L5 \times 3\frac{1}{2} \times \frac{5}{16}$	A36
19	$L4 \times 4 \times \frac{3}{8}$	A572, Grade 50
20	$L4 \times 4 \times \frac{5}{16}$	A572, Grade 50
21	$L5 \times 5 \times \frac{5}{16}$	A36
22	$L5 \times 3 \times \frac{5}{16}$	A36
23	$L2\frac{1}{2} \times 2\frac{1}{2} \times \frac{3}{16}$	A572, Grade 50
24	$L2\frac{1}{2} \times 2\frac{1}{2} \times \frac{3}{16}$	A36
25	$L2\frac{1}{2} \times 2\frac{1}{2} \times \frac{3}{16}$	A36
26	$L3 \times 3 \times \frac{3}{16}$	A36
27	$L2 \times 1\frac{1}{4} \times \frac{3}{16}$	A36
28	$L5 \times 3\frac{1}{2} \times \frac{1}{4}$	A36
29	$L3\frac{1}{2} \times 3\frac{1}{2} \times \frac{1}{4}$	A572, Grade 50
30	$L3 \times 2\frac{1}{2} \times \frac{1}{4}$	A572, Grade 50
31	$L3\frac{1}{2} \times 2\frac{1}{2} \times \frac{1}{4}$	A572, Grade 50
32	$L4 \times 3 \times \frac{1}{4}$	A572, Grade 50
33	$L4 \times 3\frac{1}{2} \times \frac{1}{4}$	A572, Grade 50
34	$L3 \times 3 \times \frac{3}{16}$	A36
35	$L2\frac{1}{2} \times 2\frac{1}{2} \times \frac{3}{16}$	A36
36	$L3 \times 3 \times \frac{3}{16}$	A36
37	$L2\frac{1}{2} \times 2 \times \frac{3}{16}$	A36

38	$L1\frac{3}{4} \times 1\frac{3}{4} \times \frac{1}{8}$	A36
39	$L2\frac{1}{2} \times 2\frac{1}{2} \times \frac{3}{16}$	A36
40	$L1\frac{3}{4} \times 1\frac{3}{4} \times \frac{3}{16}$	A36
41	Not a member	
42	$L3\frac{1}{2} \times 3 \times \frac{1}{4}$	A572, Grade 50
43	$L6 \times 6 \times \frac{7}{16}$	A572, Grade 50
44	$L2\frac{1}{2} \times 2\frac{1}{2} \times \frac{1}{4}$	A572, Grade 50
45	$L6 \times 4 \times \frac{3}{8}$	A36
46	$L2\frac{1}{2} \times 2 \times \frac{1}{4}$	A572, Grade 50
47	$L4 \times 4 \times \frac{1}{4}$	A36
48	$L3 \times 2\frac{1}{2} \times \frac{1}{4}$	A36
49	$L1\frac{3}{4} \times 1\frac{3}{4} \times \frac{1}{8}$	A36
50	$L2 \times 2 \times \frac{3}{16}$	A36
51	$L1\frac{3}{4} \times 1\frac{3}{4} \times \frac{1}{8}$	A36
52	$L1\frac{3}{4} \times 1\frac{3}{4} \times \frac{1}{8}$	A36
53	$L3\frac{1}{2} \times 2\frac{1}{2} \times \frac{1}{4}$	A36
54	$L1\frac{3}{4} \times 1\frac{1}{4} \times \frac{1}{8}$	A36
55	$L2 \times 2 \times \frac{1}{8}$	A36
56	$L1\frac{3}{4} \times 1\frac{3}{4} \times \frac{1}{8}$	A36
57	$L3\frac{1}{2} \times 2\frac{1}{2} \times \frac{1}{4}$	A36
58	$L2 \times 2 \times \frac{3}{16}$	A36
59	$L3\frac{1}{2} \times 2\frac{1}{2} \times \frac{1}{4}$	A36
60	$L2 \times 2 \times \frac{3}{16}$	A36
61	$L3 \times 2\frac{1}{2} \times \frac{1}{4}$	A36
62	$L2\frac{1}{2} \times 2 \times \frac{3}{16}$	A36
a	$L1\frac{3}{4} \times 1\frac{1}{4} \times \frac{1}{8}$	A36
b	$L1\frac{3}{4} \times 1\frac{3}{4} \times \frac{1}{8}$	A36

Notes:

1. Specifications: ASCE Manual & Report on Engineering Practice – No. 52, "Guide for Design of Steel Transmission Towers", 1971 (except minimum thickness)
2. Material: ASTM A36 and ASTM A572, Grade 50 (USS Ex-Ten 50)
3. Some cross sections in Table A.1 are not used in the tower shown in Fig. A.1, but they may be used in the body or leg extensions. These extra cross sections are given for completeness, although the drawings of the body and leg extensions are not included in Fig. A.1.
4. Ground wires: 2-7/16" R.S. Steel Max. Tension
5. Conductors: 3-795 MCM ACSR (26/7)
6. Weight span: 4,600'
7. Wind span: 4,600' with 12° Angle in Line
   3,600' with 18° Angle in Line
   2,600' with 24° Angle in Line
   1,600' with 30° Angle in Line

Table A.2. Design loads (units: kips)

Load case	Load condition	Type of loading	Loading points					Total load
			G1	G2	C1	C2	C3	

		Vert.	5.80	5.80	12.55	12.55	12.55	49.25
1	Intact	Trans.	8.14	8.14	13.52	13.52	13.52	56.84
		Long.	N.A.	N.A.	N.A.	N.A.	N.A.	N.A.
		Vert.	2.90	2.90	6.28	6.28	6.28	24.64
2	Dead end	Trans.	4.07	4.07	6.76	6.76	6.76	28.42
		Long.	11.97	11.97	20.60	20.60	20.60	85.74
		Vert.	5.80	5.80	12.55	12.55	12.55	49.25
3	3 broken conductors	Trans.	8.14	8.14	6.76	6.76	6.76	36.56
		Long.	N.A.	N.A.	20.60	20.60	20.60	61.80
		Vert.	5.80	5.80	12.55	12.55	12.55	49.25
4	1 broken ground wire & 2 broken cond.	Trans.	4.07	8.14	6.76	6.76	13.52	39.25
		Long.	11.97	N.A.	20.60	20.60	N.A.	53.17
		Vert.	5.80	5.80	12.55	12.55	12.55	49.25
5	2 broken ground wires & 1 broken cond.	Trans.	4.07	4.07	6.76	13.52	13.52	41.94
		Long.	11.97	11.97	20.60	N.A.	N.A.	44.54
		Vert.	12.85	12.85	22.03	22.03	22.03	91.79
6	Heavy vertical	Trans.	N.A.	N.A.	N.A.	N.A.	N.A.	N.A.
		Long.	N.A.	N.A.	N.A.	N.A.	N.A.	N.A.

Notes: In the fragility development process presented in this paper, the tower is assumed under "Intact" load condition, which means no longitudinal forces are transferred to the tower from the conductors and ground wires.

To validate the finite element model, the tower is analyzed using OpenSees under load cases 1 and 5. The design vertical/gravity loads are first applied to the tower, and the lateral loads are then increased proportionally to the design lateral loads until failure of the tower. Fig. A.2 shows the force-displacement relationships until failure of the tower, where the horizontal axis is the displacement at the top of the tower and the vertical axis is the ratio of the applied lateral force and the design lateral force. It is seen that the capacity of the tower is about 5% to 7% higher than the design loads.

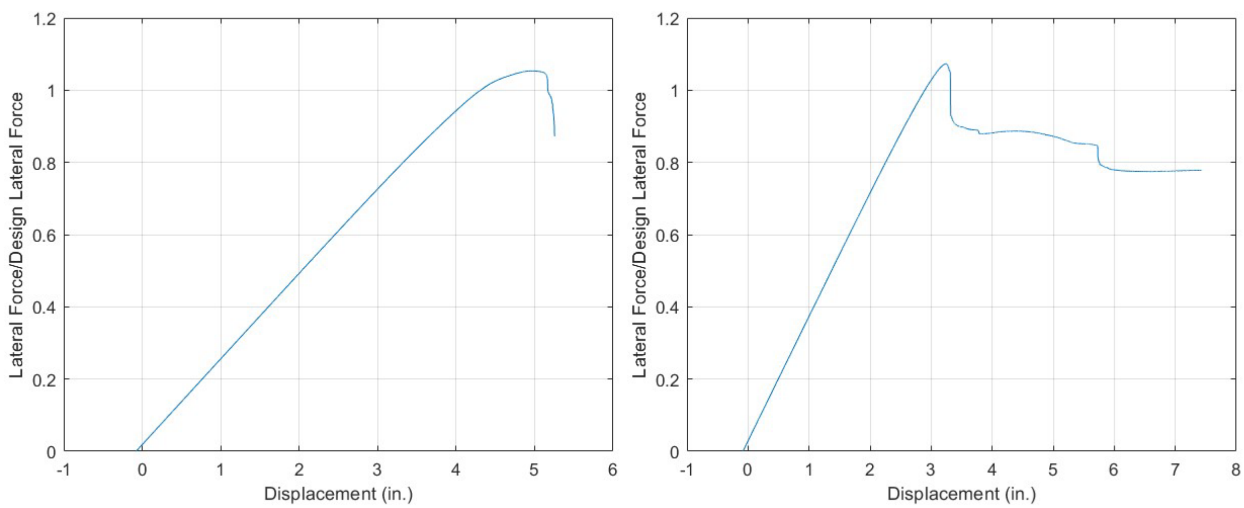

(a) Load case 1 (b) Load case 5

Fig. A.2. Force-displacement curves under two load cases

References

ASCE 2010. "Minimum Design Loads for Buildings and Other Structures (ASCE Standard 7-10)." American Society of Civil Engineers, Reston, VA.

ASCE 2016. "Minimum Design Loads and associated criteria for Buildings and Other Structures (ASCE Standard 7-16)." American Society of Civil Engineers, Reston, VA.

ASCE 2020. "Guidelines for electrical transmission line structural loading." American Society of Civil Engineers, Reston, VA.

ASCE 2023. "Prestandard for Performance-Based Wind Design V1.1." American Society of Civil Engineers, Reston, VA.

Baker, J. W. 2015. "Efficient analytical fragility function fitting using dynamic structural analysis." *Earthquake Spectra*, 31(1), 579-599.

Banik, S., Hong, H., and Kopp, G. A. 2010. "Assessment of capacity curves for transmission line towers under wind loading." *Wind & structures*, 13(1), 1-20.

Barbato, M., Petrini, F., Unnikrishnan, V. U., and Ciampoli, M. 2013. "Performance-based hurricane engineering (PBHE) framework." *Structural Safety*, 45, 24-35.

Cai, Y., Xie, Q., Xue, S., Hu, L., and Kareem, A. 2019. "Fragility modelling framework for transmission line towers under winds." *Engineering Structures*, 191, 686-697.

Cheynet, E. 2020. "Wind field simulation (the user-friendly version)." Accessed May 24, 2020. https://www.github.com/ECheynet/windSim_textBased.

Chuang, W.-C., and Spence, S. M. 2019. "An efficient framework for the inelastic performance assessment of structural systems subject to stochastic wind loads." *Engineering Structures*, 179, 92-105.

Chuang, W.-C., and Spence, S. M. 2020. "Probabilistic performance assessment of inelastic wind excited structures within the setting of distributed plasticity." *Structural Safety*, 84, 101923.

Darestani, Y. M., Jeddi, A. B., and Shafieezadeh, A. 2022. Hurricane Fragility Assessment of Power Transmission Towers for a New Set of Performance-Based Limit States. In *Engineering for Extremes* (pp. 167-188): Springer.

Davenport, A. G. 1961. "The spectrum of horizontal gustiness near the ground in high winds." *Quarterly Journal of the Royal Meteorological Society*, 87(372), 194-211.

Deodatis, G. 1996. "Simulation of ergodic multivariate stochastic processes." *Journal of engineering mechanics*, 122(8), 778-787.

Der Kiureghian, A. 2005. First-and second-order reliability methods. In E. Nikolaidis, D. Ghiocel, and S. Singhal (Eds.), *Engineering design reliability handbook*. Boca Raton, FL: CRC Press.

Du, X., and Hajjar, J. F. 2021a. "Three-dimensional nonlinear displacement-based beam element for members with angle and tee sections." *Engineering Structures*, 239, 112239.

Du, X., and Hajjar, J. F. 2021b. "Three-dimensional nonlinear mixed 6-DOF beam element for thin-walled members." *Thin-Walled Structures*, 164, 107817.

Du, X., and Hajjar, J. F. 2022. "Hurricane fragility analysis of electrical transmission towers." *The Electrical Transmission and Substation Structures Conference*, American Society of Civil Engineers, Orlando, FL.

Du, X., Hajjar, J. F., Bond, R. B., Ren, P., and Sun, H. 2023. "Clustering and Selection of Hurricane Wind Records Using Autoencoder and k-Means Algorithm." *Journal of Structural Engineering*, 149(8), 04023096.

Ellingwood, B. R., Rosowsky, D. V., Li, Y., and Kim, J. H. 2004. "Fragility assessment of light-frame wood construction subjected to wind and earthquake hazards." *Journal of Structural Engineering*, 130(12), 1921-1930.

Fritsch, F. N., and Carlson, R. E. 1980. "Monotone piecewise cubic interpolation." *SIAM Journal on Numerical Analysis*, 17(2), 238-246.

Fu, X., Li, H.-N., and Li, G. 2016. "Fragility analysis and estimation of collapse status for transmission tower subjected to wind and rain loads." *Structural safety*, 58, 1-10.

Fu, X., Li, H.-N., Li, G., and Dong, Z.-Q. 2020. "Fragility analysis of a transmission tower under combined wind and rain loads." *Journal of Wind Engineering and Industrial Aerodynamics*, 199, 104098.

Hallowell, S. T., Myers, A. T., Arwade, S. R., Pang, W., Rawal, P., Hines, E. M., Hajjar, J. F., Qiao, C., Valamanesh, V., and Wei, K. 2018. "Hurricane risk assessment of offshore wind turbines." *Renewable Energy*, 125, 234-249.

HIFLD 2018. "Homeland Infrastructure Foundation-Level Data (HIFLD)." Accessed April 26, 2018. https://hifld-geoplatform.opendata.arcgis.com/.

Ibarra, L. F., and Krawinkler, H. 2005. *Global collapse of frame structures under seismic excitations*. Stanford, CA: John A. Blume Earthquake Engineering Center.

Kahaner, D., Moler, C., and Nash, S. 1989. *Numerical methods and software*: Prentice-Hall, Inc.

Kaimal, J. C., Wyngaard, J., Izumi, Y., and Coté, O. 1972. "Spectral characteristics of surface‐layer turbulence." *Quarterly Journal of the Royal Meteorological Society*, 98(417), 563-589.

Kim, D.-S., Ok, S.-Y., Song, J., and Koh, H.-M. 2013. "System reliability analysis using dominant failure modes identified by selective searching technique." *Reliability Engineering & System Safety*, 119, 316-331.

Kim, S.-M., Ok, S.-Y., and Song, J. 2019. "Multi-scale dynamic system reliability analysis of actively-controlled structures under random stationary ground motions." *KSCE Journal of Civil Engineering*, 23(3), 1259-1270.

Kitipornchai, S., and Lee, H. 1986. "Inelastic buckling of single-angle, tee and double-angle struts." *Journal of Constructional Steel Research*, 6(1), 3-20.

Li, Y. 2005. "Fragility methodology for performance-based engineering of wood-frame residential construction." PhD Dissertation, Georgia Institute of Technology, Atlanta, GA.

Li, Y., and Ellingwood, B. R. 2006. "Hurricane damage to residential construction in the US: Importance of uncertainty modeling in risk assessment." *Engineering structures*, 28(7), 1009-1018.

Liu, F. 2014. "Projections of future US design wind speeds and hurricane losses due to climate change." PhD Dissertation, Clemson University, Clemson, SC.

Liu, Y., and Hui, L. 2008. "Experimental study of beam–column behaviour of steel single angles." *Journal of Constructional Steel Research*, 64(5), 505-514.

Ma, L., Khazaali, M., and Bocchini, P. 2021. "Component-based fragility analysis of transmission towers subjected to hurricane wind load." *Engineering Structures*, 242, 112586.

Mara, T. G. 2013. "Capacity assessment of a transmission tower under wind loading." PhD Dissertation, The University of Western Ontario, London, Ontario, Canada.

MathWorks 2022. "MATLAB Documentation." Accessed May 16, 2022, 2022. https://www.mathworks.com/help/matlab/ref/interp1.html#btwp6lt-3.

McKenna, F., Scott, M. H., and Fenves, G. L. 2010. "Nonlinear finite-element analysis software architecture using object composition." *Journal of Computing in Civil Engineering*, 24(1), 95-107.

Rathje, E. M., Dawson, C., Padgett, J. E., Pinelli, J.-P., Stanzione, D., Adair, A., Arduino, P., Brandenberg, S. J., Cockerill, T., and Dey, C. 2017. "DesignSafe: New cyberinfrastructure for natural hazards engineering." *Natural Hazards Review*, 18(3), 06017001.

Shafieezadeh, A., Onyewuchi, U. P., Begovic, M. M., and DesRoches, R. 2013. "Age-dependent fragility models of utility wood poles in power distribution networks against extreme wind hazards." *IEEE Transactions on Power Delivery*, 29(1), 131-139.

Shanmugam, B. 2011. "Probablistic assessment of roof uplift capacities in low-rise residential construction." PhD Dissertation, Clemson University, Clemson, South Carolina, USA.

Shinozuka, M. 1972. "Monte Carlo solution of structural dynamics." *Computers & Structures*, 2(5-6), 855-874.

Shinozuka, M., Feng, M. Q., Lee, J., and Naganuma, T. 2000. "Statistical analysis of fragility curves." *Journal of engineering mechanics*, 126(12), 1224-1231.

Shinozuka, M., and Jan, C.-M. 1972. "Digital simulation of random processes and its applications." *Journal of sound and vibration*, 25(1), 111-128.

Simiu, E., Patel, V., and Nash, J. 1974. "Mean wind profiles in hurricanes." *JOURNAL OF ENINEERING MECHANICS DVISION ASCE*, 100, 833-837.

Simiu, E., Patel, V., and Nash, J. F. 1976. "Mean speed profiles of hurricane winds." *Journal of the Engineering Mechanics Division*, 102(2), 265-273.

Simiu, E., and Scanlan, R. H. 1996. *Wind effects on structures: fundamentals and applications to design* (3rd ed.). New York, NY: John Wiley & Sons, Inc.

Song, J., and Ok, S. Y. 2010. "Multi‐scale system reliability analysis of lifeline networks under earthquake hazards." *Earthquake engineering & structural dynamics*, 39(3), 259-279.

Straub, D., Schneider, R., Bismut, E., and Kim, H.-J. 2020. "Reliability analysis of deteriorating structural systems." *Structural safety*, 82, 101877.

Tian, L., Zhang, X., and Fu, X. 2020. "Fragility analysis of a long-span transmission tower–line system under wind loads." *Advances in Structural Engineering*, 23(10), 2110-2120.

Vamvatsikos, D., and Cornell, C. A. 2002. "Incremental dynamic analysis." *Earthquake Engineering & Structural Dynamics*, 31(3), 491-514.

Vamvatsikos, D., and Cornell, C. A. 2004. "Applied incremental dynamic analysis." *Earthquake spectra*, 20(2), 523-553.

Vamvatsikos, D., Jalayer, F., and Cornell, C. A. "Application of incremental dynamic analysis to an RC-structure." In *Proc., Proceedings of the FIB symposium on concrete structures in seismic regions*, 75-86.

Zhang, W., Zhu, J., Liu, H., and Niu, H. 2015. "Probabilistic capacity assessment of lattice transmission towers under strong wind." *Frontiers in Built Environment*, 1, 20.